PHILOSOPHICAL TRANSACTIONS OF THE ROYAL SOCIETY A

rsta.royalsocietypublishing.org

Review

Cite this article: Armstrong RW. 2014 Bertram Hopkinson's pioneering work and the dislocation mechanics of high rate deformations and mechanically induced detonations. *Phil. Trans. R. Soc. A* **372**: 20130181. http://dx.doi.org/10.1098/rsta.2013.0181

One contribution of 12 to a Theme Issue 'Shock and blast: a celebration of the centenary of Bertram Hopkinson's seminal paper of 1914 (Part 1)'.

Subject Areas:
mechanics, solid state physics

Keywords:
dislocation-mechanics-based constitutive relations, shock-induced deformations, isentropic compression, dislocation pile-up avalanches, detonation, shear banding

Author for correspondence:
Ronald W. Armstrong
e-mail: rona@umd.edu

Bertram Hopkinson's pioneering work and the dislocation mechanics of high rate deformations and mechanically induced detonations

Ronald W. Armstrong

Center for Energetic Concepts Development, Department of Mechanical Engineering, University of Maryland, College Park, MD 21842, USA

Bertram Hopkinson was prescient in writing of the importance of better measuring, albeit better understanding, the nature of high rate deformation of materials in general and, in particular, of the importance of heat in initiating detonation of explosives. This report deals with these subjects in terms of post-Hopkinson crystal dislocation mechanics applied to high rate deformations, including impact tests, Hopkinson pressure bar results, Zerilli–Armstrong-type constitutive relations, shock-induced deformations, isentropic compression experiments, mechanical initiation of explosive crystals and shear banding in metals.

1. Introduction

An early introduction of the present author to split-Hopkinson pressure bar (SHPB) testing was provided by Harry Kolsky [1]. Kolsky had employed the SHPB to study the dynamic fracture of glass and polymeric solids with end-of-bar reflected tensile waves. The same technique was employed to achieve basal plane cleavage stresses exceeding 160 MPa for [0001] axis-direction cylindrical single crystal bars of zinc. The influence of pre-cleavage plastic flow was minimized in the tests. Hopkinson had described the tensile wave conversion on reflection of a compressive wave [2]. Modern reports

Royal Society Publishing

have described direct use of a split-Hopkinson tension bar [3] and a split-Hopkinson tension bar modification employing a 'U-shaped' striker bar as projectile to produce virtually oscillation-free square pulses [4].

Later connection of the present author and colleagues was with SHPB plasticity results obtained on copper and showing an upturn in the material strength at dynamic deformation rates exceeding approximately $10^3\ s^{-1}$, as will be described in this report in relation to higher rate comparisons with shock and isentropic compression experiments (ICEs) also done on copper. In the same connection, an analysis of important shock results obtained on Armco iron materials at different grain sizes is to be described [5].

Hopkinson had reported early results on detonation-induced (back-side) spalling of mild steel material and this behaviour is to be connected here with modern spall results and modelling of them. And lastly, there is consideration of the influence of plastic deformation on shear banding that is associated with localized adiabatic heating and the initiation of detonation in energetic crystals, this relating to Hopkinson's concern with the critical influence of heat (or temperature) in promoting chemical decomposition of gun-cotton [6]. An interesting point in Hopkinson's 1914 report is a schematic picture of a flattened lead bullet relating to calculations of such generated pressures [7]. The test result can be taken without too much imagination to presage Taylor's solid cylinder impact test for determining the dynamic yield strength of mild steel [8].

This review begins, first, with impact test results and coupled constitutive relation descriptions. Different yield conditions for body-centred cubic (BCC) slip and deformation twinning are described for steel and Armco iron materials [9]. Then another somewhat different constitutive deformation behaviour, which is focused on the temperature and strain rate dependence of strain hardening for face-centred cubic (FCC) copper, is described [10]. The constitutive modelling is related to other deformations including spall-related spherical impacts on copper [11]. Very different strength levels obtained in shock versus ICE results are described for copper. For Armco iron, a twinning-determined grain-size dependence of the Hugoniot elastic limit (HEL) stress is shown to disappear for good reason in the subsequent plastic flow stress dependence on strain rate [5]. The grain-size dependence is explained in terms of dislocation pile-ups. The sudden release of a pile-up provides a fundamental explanation of shear banding behaviour in the high rate deformation behaviour of metals [12]. Such dislocation pile-up avalanches have been employed also to explain greater drop-weight heights being required to initiate chemical decomposition of smaller explosive crystals [13].

2. Taylor impact test results on mild steel and Armco iron

Taylor provided an analysis by which the average dynamic yield strength of a metal could be determined from the length change of a solid cylinder after impacting onto a rigid target [8]; and colleague, Wiffen [14], demonstrated application of the method to impact results obtained for a variety of materials. Included in the project was a study by Carrington & Gaylor [15] of the hardness properties measured at various positions along the longitudinal section of an impacted mild steel specimen, as shown in figure 1. Much later, Johnson & Cook [16] employed such Taylor-type impact results in developing numerical relations for application in the elastic plastic impact computation (EPIC) code. At that time until the present, a major effort, with advancement in such hydrocode descriptions, is to compute the complete deformation shape of Taylor and other type impacted specimens. Zerilli & Armstrong [17] followed on from Johnson and Cook with development of dislocation mechanics based constitutive relations, now known as the Z–A equations, for material dynamics calculations.

A Z–A-type relation for the flow stress, σ_ε, of Armco iron and related BCC metals and alloys was obtained in the form

$$\sigma_\varepsilon = \sigma_G + B_0 \exp\left\{\left[-\beta_0 + \beta_1 \ln\left(\frac{d\varepsilon}{dt}\right)\right] T\right\} + K\varepsilon^n + k_\varepsilon \ell^{-1/2}. \tag{2.1}$$

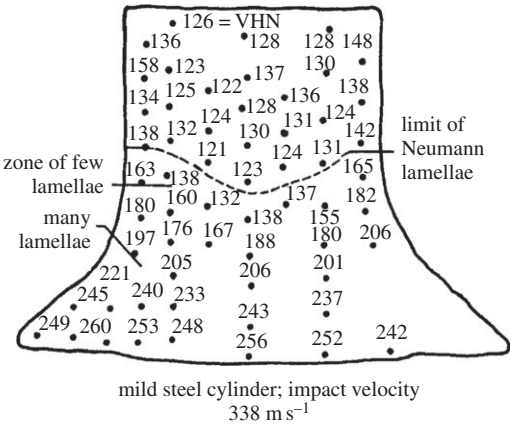

Figure 1. Longitudinal section of a Taylor impact specimen with local post-impact Vickers hardness numbers (VHNs) listed at the indicated positions to demonstrate a greater hardness within the zone of induced deformation twinning (Neumann banding).

In the physical model development of equation (2.1), σ_G is an athermal stress component determined by the presence of solute, precipitates and an initial dislocation density; B_0 is a reference stress at temperature $T = 0\,\mathrm{K}$; β_0 and β_1 are exponential temperature coefficients, including the effect of strain rate ($\mathrm{d}\varepsilon/\mathrm{d}t$); K and n apply for power law strain hardening; k_ε is a microstructural stress intensity; and ℓ is the average polycrystal grain diameter, i.e. generally determined on a line-intercept basis. Most often, the first three terms on the right-hand side of equation (2.1) are combined into a single 'friction stress', $\sigma_{0\varepsilon}$, for the plastic flow of the average polycrystal grain volume and when added to the $k_\varepsilon \ell^{-1/2}$ term is known eponymously as the Hall–Petch (H–P) relation that was determined from measurements made of the yield and cleavage stresses of iron and steel materials [18–20]. The major temperature and strain rate dependence in equation (2.1) was shown to produce reasonably constant values of B_0, β_0 and β_1 for different steel materials [21].

(a) The role of deformation twinning

Direct employment of equation (2.1) in the EPIC code led to prediction of the deformed specimen being softer than the measured shape, particularly at the impact end, and deformation twinning was held to be responsible [17]. Twinning was incorporated into the EPIC calculation by employment of an H–P-type deformation twinning relation

$$\sigma_T = \sigma_{0T} + k_T \ell^{-1/2}, \tag{2.2}$$

where σ_{0T} is a micro-slip friction stress associated with the local stress intensity, k_T, required for twin nucleation at grain boundaries; $k_T \sim 90\,\mathrm{MPa\,mm^{1/2}}$ for twinning as compared with $k_\varepsilon \sim 22\,\mathrm{MPa\,mm^{1/2}}$ for slip. Figure 2 shows the excellent match of computed and experimental result when twinning was taken into account [22].

(b) The time dependence

The hardening produced by deformation twinning was attributed to a reduction in grain size immediately caused by the new twin interfaces producing similar obstacles to slip as for grain boundaries. Examination of the sectioned Armco iron specimen showed that approximately four twins per grain were produced when twinning occurred and a reduction in grain size was estimated [22]. Further investigation of the time sequence for twinning and slip was carried out within the EPIC code as shown in figure 3 for which the sequential development of the interface between twinned and twin-free material, at 'A', could be followed [23]. Very interestingly, the

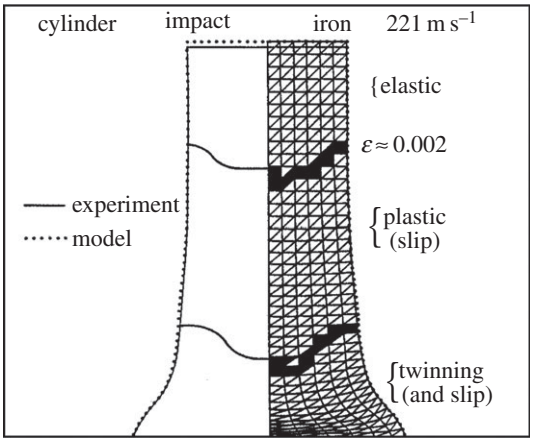

Figure 2. Experimental Taylor test result of Johnson & Cook [16] for Armco iron.

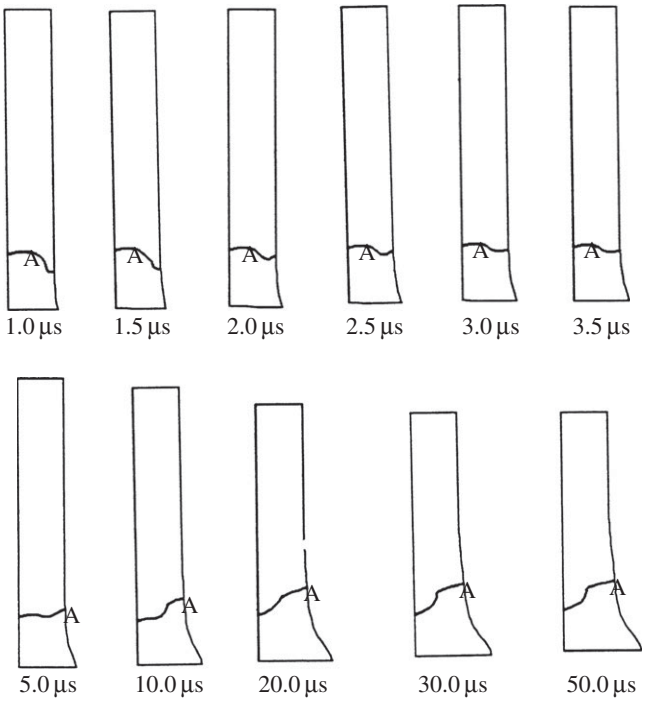

Figure 3. Time sequence for EPIC-modelled twinning versus slip in Armco iron.

initial twinning that occurred within approximately 1 μs produced a convex interface at A that subsequently changed over a time period of approximately 50 μs, because of the follow-on deformation by slip, to a concave shape in agreement with the mild steel interface shown in figure 1. The times compare favourably with Hopkinson's measurements of approximately 20–60 μs for the individual cases of completion of bullet impacts or full lifetimes of detonation pressures [6,7]. And very importantly, one could regard the effect of the deformation twinning in the sequential stages just described as producing a new hardened front-end of the bar that then was to be deformed by slip.

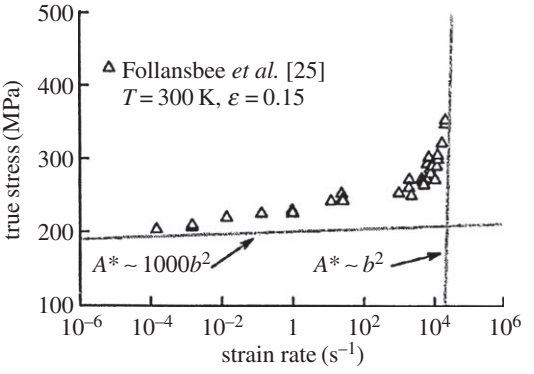

Figure 4. SHPB measurements of the strain rate dependence of the flow stress of OFE copper.

3. Dislocation dynamics for several copper results

Taylor test results reported by Johnson & Cook [16] for copper material were shown to be closely matched (in the absence of any deformation twinning) with code computations made for an FCC-structure-based Z–A relation of the form [17]

$$\sigma = \sigma_G + B_0 \left\{ \varepsilon_r \left[1 - \exp\left(\frac{-\varepsilon}{\varepsilon_r} \right) \right] \right\}^{1/2} \exp\left[-\alpha_0 + \alpha_1 \ln\left(\frac{d\varepsilon}{dt} \right) \right] + k_\varepsilon \ell^{-1/2}, \tag{3.1}$$

where σ_G has the same explanation as for the BCC case but, for the next term, the temperature and strain rate characterized coefficients B_0, α_0 and α_1 apply for a dislocation modelled strain-hardening behaviour that is moderated at larger strains by ε_r. At smaller strains, the stress–strain curve approximates to a parabolic dependence [24]. A lower $k_\varepsilon = 5\,\mathrm{MPa\,mm^{1/2}}$ applies for copper. With Z–A constants determined from other reference test results, the closely modelled Taylor test shape was shown to involve a range of true strains of $0 \le \varepsilon \le 1.5$, strain rates of $0 \le (d\varepsilon/dt) \le \sim 10^5\,s^{-1}$ and $300 \le T \le 600\,K$.

In contrast with agreement being reported on a Z–A basis for the copper Taylor test result [17], figure 4 shows a somewhat surprisingly strong upturn at the high strain rate end of SHPB flow stress measurements reported by Follansbee *et al*. [25], in testing of oxygen-free electronic (OFE) copper material. In the figure, tangent slopes are shown at both lower and higher $(d\varepsilon/dt)$ values to indicate activation area dimensions, A^*, specified for a thermal stress dependence according to the relationship

$$A^* = \left(\frac{kT}{b} \right) \left(\frac{\partial [\ln(d\gamma/dt)]}{\partial \tau_{Th}} \right)_T, \tag{3.2}$$

where k is Boltzmann's constant; b is dislocation Burgers vector; $(d\gamma/dt) = m(d\varepsilon/dt)$, in which $m = 3.1$ is the Taylor factor for transformation of strains among the five independent slip systems of the polycrystal grains [24]; and $\tau_{Th} = (\sigma_\varepsilon - \sigma_G)/m$. Values of $100 \le A^* \le 1000b^2$ are typical of plastic flow controlled within FCC metals by the intersection of dislocations [26]. Of additional interest in connection with relationship of Hopkinson and Taylor researches is a report by Volterra who described experimental results obtained on a proprietary polymeric material via a Hopkinson bar test system constructed at Cambridge and whose deformation curve approximated to a parabolic flow stress dependence on strain [27].

(a) Evidence for dislocation generation

Follansbee *et al*. [25] put forward the consideration that dislocation drag (resistance between thermally activated obstacles) was responsible for the upturn in flow stress dependence. However, the severe reduction in A^* indicated in figure 4 favours a strong increase in generation of an enhanced dislocation density. An increase in the dislocation density is more in line with

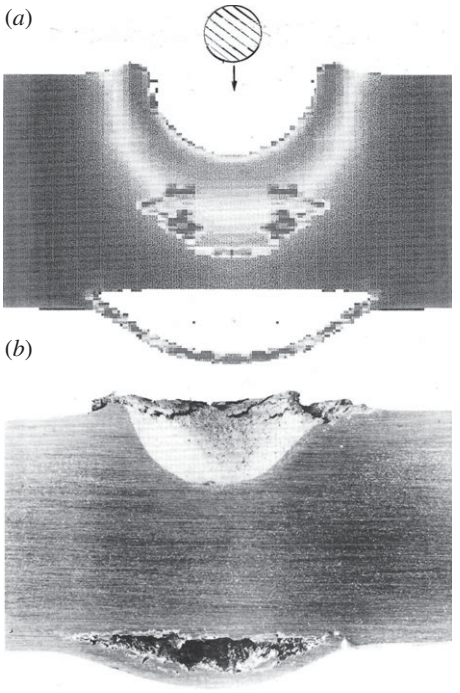

Figure 5. (*a*) Model and (*b*) experiment for spherical aluminium impact on a copper target [30].

corresponding measurements reported for an increase in the material ductility through a larger uniform strain to the maximum load point. And later connection to be made here between these flow stress measurements and pioneering results reported for shock-determined plastic flow stresses is in agreement with the upturn being attributed to an enhanced dislocation generation. Nevertheless, the issue is still undecided. For example, Cai *et al.* [28] have provided a close match of the Follansbee *et al.* results and model description of them based both on a drag-modified Z–A type description and on a new relationship. Fan *et al.* [29] have suggested that such an upturn may be a result of non-thermal effect entering at high strain rate.

(b) Spall test results

Hopkinson's pioneering interest in back-side spall caused by dynamic loading [8] has a modern counterpart in modelling of the impact penetration experiment shown in figure 5 [31]. In the figure, a Eulerian autodyne code computation involving the Johnson–Cook numerical relations is shown for comparison with a crater shape and spall produced by gas gun propelled impact of a 3.16 mm diameter 1100 aluminium alloy sphere onto a 1.3 cm thick oxygen-free high conductivity copper plate. The impact velocity was 6.01 km s^{-1} and was modelled on a microsecond time scale. Hopkinson commented on such spall-type cracking produced in mild steel plates by the detonation of gun-cotton compacts and described the results as being comparable to those achieved by bullet impacts [6]. Murr [30] has produced an extensive review of microstructures developed by different types of impact penetrations that also were monitored by performing local post-impact hardness measurements in the same manner as employed by Carrington & Gaylor [15].

4. Dislocation generation in shocks versus isentropic compression experiments

Consideration of a nanoscale dislocation structure being generated at a propagating shock front brings forth again the issue of a limiting small activation area at the atomic level [32].

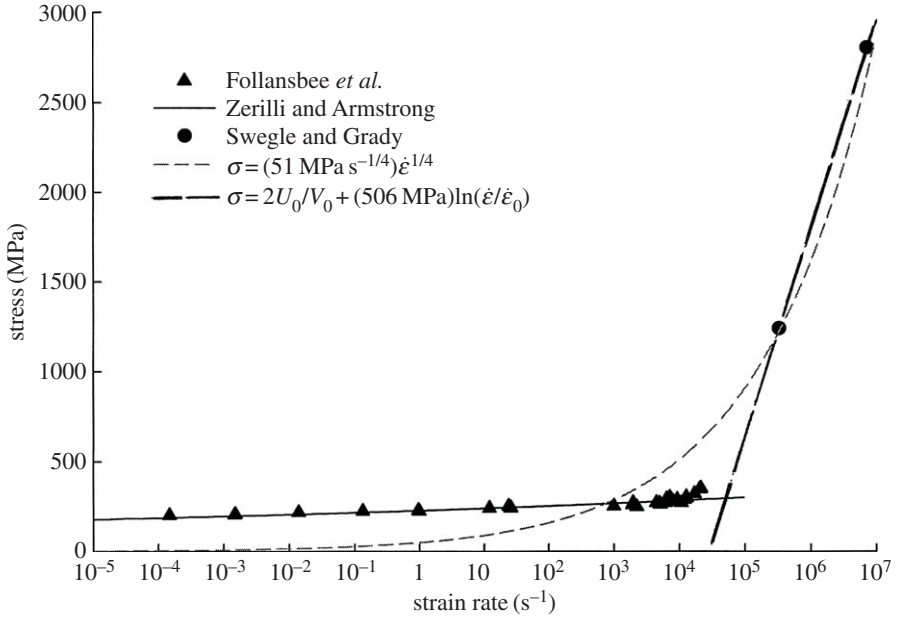

Figure 6. Comparison of SHPB and shock results for OFE copper.

Armstrong *et al*. [5] extended the Z–A-type dislocation mechanics analysis to consider the case for which a smallest limiting value of A^* should be applicable for determining the magnitude of the unidirectional shock stress, σ_S, and proposed such model connection with shock-induced deformation for which a post-shock state of one-dimensional strain might be achieved. The rather simple constitutive relationship was obtained

$$\sigma_S = \left(\frac{2G_{0G}}{b^3}\right) - \left(\frac{2kT}{b^3}\right) \ln\left[\frac{(d\varepsilon/dt)_{0G}}{(d\varepsilon/dt)}\right], \tag{4.1}$$

where G_{0G} is the reference Gibbs free energy for dislocation generation and $(d\varepsilon/dt)_{0G}$ is the upper limiting strain rate for the process.

(a) Comparison with Swegle and Grady results for copper

Figure 6 shows at a different ordinate scale the Follansbee *et al*. SHPB results for copper in comparison with pioneering shock measurements reported by Swegle & Grady [33] and, also, with application of several constitutive relations. The lower line is the Z–A prediction from equation (3.1). The short-dashed line is a (1/4) power relationship developed by Swegle and Grady. The nearly vertical long-dashed line is equation (4.1) fitted to the Swegle and Grady results. Evaluation of the slope value $(2kT/b^3)$ gives $b = 0.255$ nm in remarkable agreement with the known Burgers vector for unit slip in copper.

(b) Grain-size aspects of Arnold results for Armco iron

Arnold obtained comprehensive shock results at different grain sizes on Armco iron material [34]. The measurements have provided another example to compare with model prediction. Figure 7 illustrates an important aspect of the resultant grain-size dependence, or its absence, for test results obtained for three grain sizes. The closely spaced curves shown at the foot of the figure followed results obtained in SHPB tests as matched with the Z–A relationship from equation (2.1). The encompassing three horizontal lines are the computed deformation twinning stresses obtained from equation (2.2). The filled square, triangle and inverted triangle points are

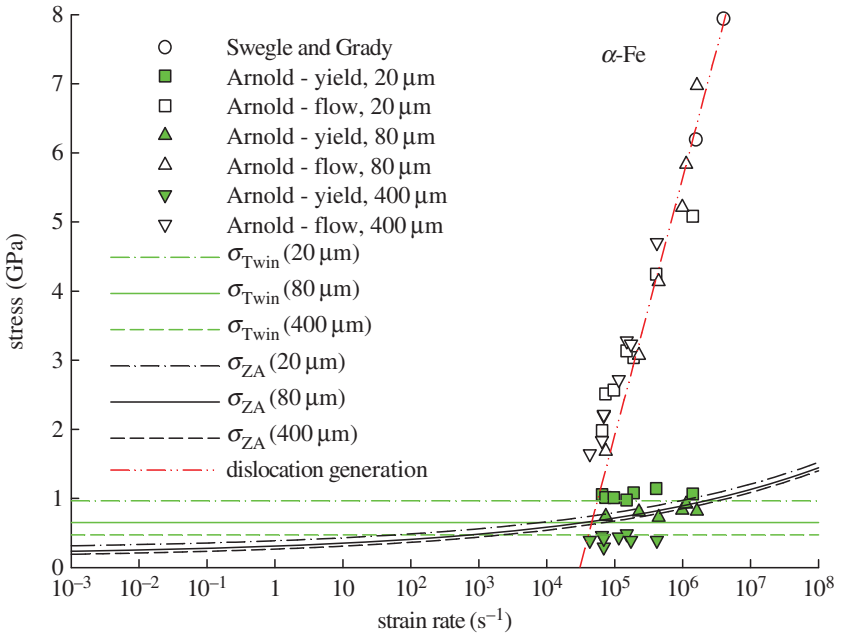

Figure 7. Shock results for Armco iron at different grain sizes. (Online version in colour.)

for the determined HEL stresses. The points show that the HEL corresponds to the onset of deformation twinning and give reasonable verification of the athermal nature of the twinning stress. The close proximity of the Z–A slip and H–P twinning stresses at the operative strain rates is in line with the material being in the region of the ductile–brittle transition as was referenced above [21]. The nearly vertical dot-and-dashed line, which includes both Arnold [34] and Swegle & Grady [33] results, has been fitted with equation (4.1) that gives in this case a value of $b^3/3$ that was matched with a double partial Burgers vector for nucleation of nanoscale twinning at the shock front [5]. The lack of grain-size dependence for the shock results is explained by plastic deformation being generated at nanoscale dimensions at the lattice points along the propagating shock front.

(c) Isentropic compression results for copper

Relatively more recent ICE testing has been developed whereby uniform loading may be accomplished sufficiently rapidly to achieve stress levels comparable to those generated in shocks. Such testing presents a different physical situation from that described for shock-induced deformations. Armstrong *et al*. [5] have pointed out that the situation for ICE should involve plastic deformation being largely controlled by the initially resident dislocation density. The required dislocation velocities do necessitate in this situation the inclusion of dislocation drag into the predicted strain rate; thus, a modification of the conventional Z–A description for the thermal stress is obtained in the form

$$\sigma_{\mathrm{Th}} = B\exp(-\beta T)\left[1 - c\left\{\frac{\mathrm{d}\varepsilon/\mathrm{d}t}{\beta_1\sigma_{\mathrm{Th}}}\right\}\right]^{-\beta 1T}, \tag{4.2}$$

where v is the dislocation velocity and c is a measure of the drag resistance specified in terms of a drag coefficient, c_0, as

$$c = \frac{c_0 m^2 \beta_1}{\rho b^2}. \tag{4.3}$$

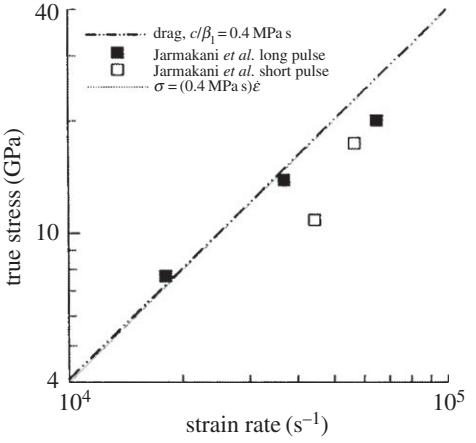

Figure 8. Comparison of ICE results and drag-modified Z–A prediction for copper.

With $\tau_{\text{Th}} = c_0 v/b$, then a linear dependence of the thermal stress on strain rate is obtained as

$$\sigma_{\text{Th}} = \left(\frac{c}{\beta_1}\right)\left(\frac{\mathrm{d}\varepsilon}{\mathrm{d}t}\right). \tag{4.4}$$

Figure 8 shows a comparison of the predicted dependence of thermal stress on strain rate and experimental results obtained in quasi-ICE gas gun tests performed on copper [35]. At these strength levels, the other terms in equation (2.1) can be neglected. The derived value of $c_0 = 8 \times 10^{-4}$ Pa s is higher than other measurements reported for $c_0 = (1\text{–}8) \times 10^{-5}$ Pa s for orders of magnitude smaller strain rates and was attributed to an increase in drag coefficient for the dislocation velocity when near to the shear wave speed [5].

5. Dislocation pile-up avalanches

One could hardly imagine without presentation of evidence that the H–P grain-size dependence and dislocation pile-up model proposed for equations (2.1)–(3.1), including the description of HEL results in figure 7, might also connect with Hopkinson's concern [6,7] for heat generated during rapid mechanical loading and leading to subsequent detonation of an energetic material. However, figure 9 shows a model consideration for the development of intense localized heating at a pile-up avalanche on breaking through a grain boundary or other suitable obstacle.

In the figure, sequential stages are shown for a local build-up of shear stress and its subsequent release, as follows: in figure 9*a* there is an initial formation of a dislocation pile-up of n_1 dislocations acting under an effective applied shear stress, $\tau_1 = \tau_{\text{a}1} - \tau_0$, in which τ_{a} is the applied shear stress and τ_0 is the slip plane friction resistance; then at the stage shown in figure 9*b*, under an increasing effective stress, τ_2, reaching a higher critical value of local shear stress concentration from n_2 dislocations bearing on the obstacle; and at $n_2\tau_2 = \tau_{\text{C}}^*$, the obstacle collapses and the pile-up is released, as indicated in figure 9*c*. The build-up mechanism and breakthrough avalanche is matched in figure 9*d* to a schematic impact pressure curve. Sudden localization of plastic work and adiabatic heating is promoted in the avalanching process because the released dislocations are driven by the concentrated shear stress at the pile-up tip [36]. Heavens & Field [37] had earlier indicated that initiation of detonation was promoted for materials exhibiting discontinuous loading in drop-weight impact tests.

(a) Initiation of detonation in explosive crystals

The model consideration shown in figure 9 was developed by Armstrong *et al.* [38] in an effort to account for evidence accumulated in the literature of 'hot spot' temperature rises occurring during

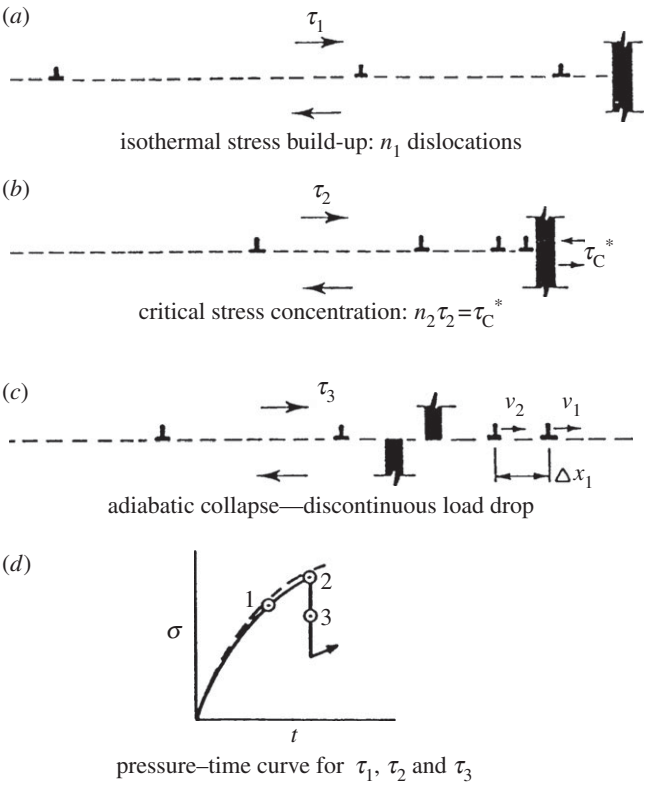

Figure 9. Schematic dislocation pile-up avalanche model for adiabatic heating.

rapid plastic deformation, particularly as would be involved in drop-weight impact testing. A relationship for the temperature rise, ΔT, for the mechanism described in figure 7 was obtained for an explosive material in the expression

$$\Delta T \geq \left(\frac{k_S \ell^{1/2}}{16\pi}\right)\left(\frac{2v}{c^* bK^*}\right)^{1/2}, \tag{5.1}$$

where k_S is the H–P shear stress intensity for obstacle collapse, v is dislocation velocity, c^* is specific heat at constant volume and K^* is thermal conductivity. Very importantly, the temperature rise is predicted to be greater for a larger grain (or crystal) size. With employment of the dislocation velocity being thermally activated and the value of stress being dependent on drop-weight height for 50% probability of initiation, H_{50}, a predicted dependence of H_{50} on crystal size was obtained for impact of a loose bed of crystals as [39]

$$H_{50} \approx \left(\frac{nk_S T}{W_0}\right)\log[f\{\Delta T, T, \ldots\}\ell^{-1/2}], \tag{5.2}$$

where n is a power exponent for the stress dependence on drop-weight height, $W_0 = \tau_{Th} bA^*$ is a constant and f is the indicated function of ΔT, T and other lesser variables all multiplied by the reciprocal square root of the grain or crystal size. In line with equation (5.2), figure 10 gives a compilation of drop-weight impact results showing agreement for a number of high explosives [40].

In figure 10, RDX is cyclotrimethylenetrinitramine, $(CH_2–N–NO_2)_3$, explosives tested at the Naval Surface Weapons Center (NAVSWC) and at the Naval Weapons Center (NWC), CL-12 is the molecular compound $(NH_2–C_6–[NO_2]_4)_2$, and HNIW is ε-hexanitrohexaazaisoisowurtzitane, known as CL-20. The material science aspects of such explosive materials have been described

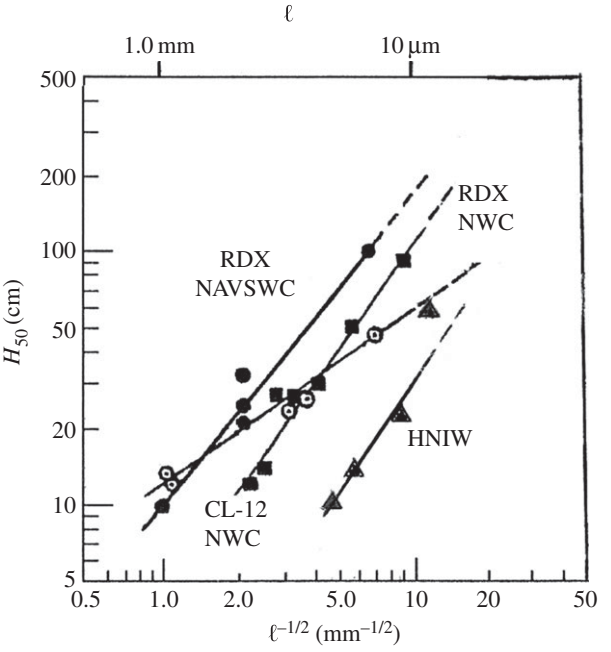

Figure 10. Drop-weight impact results obtained as a function of crystal size.

with particular emphasis given to the reduced sensitivity to mechanical loading predicted for finer material crystal sizes, whether employed individually or, more often, in composite formulations [41].

(b) Shear banding in metals

The model consideration for adiabatic heating at a dislocation pile-up avalanche led to a somewhat different description for the temperature rise, ΔT, to be expected for pile-up release in a metal system, as follows [38]:

$$\Delta T \leq \left(\frac{k_S \ell^{1/2} v}{16\pi K^*}\right) \ln\left(\frac{2K^*}{c^* v b}\right). \tag{5.3}$$

Again, as for equation (5.1), a greater temperature rise is associated with a larger grain size. Armstrong & Elban [42] reported a tabulation of temperature rises predicted for a number of explosives and metals according to equations (5.1) and (5.3). An upper limiting value of k_S was taken as the pile-up shear stress needed to produce a double Burgers vector dislocation. Such value of k_S is known to approximate well to the stress necessary for cleavage fracturing. In addition, it was noted for equation (5.3) that, except for the dislocation velocity, v, the two material-sensitive parameters determining ΔT are in the ratio k_S/K^*. Figure 11 shows a graph of k_S versus K^*, taking v as the shear wave speed for the different metals.

The right-hand ordinate scale in figure 11, when divided by K^*, may be seen to give for ordinate slope values to the individual filled-circle points the computed values of ΔT. Clearly, such values are overestimated because of v having been taken as the elastic shear wave speed. A reduction in v by two orders of magnitude would be more realistic for actual dislocation velocities and then the values of ΔT might be taken as more reasonable. Otherwise, the relative positions of the points for the different metals are in line with experience. For example, evidence has been presented of a localized molten metal spray produced in shear plugging experiments performed on Ti6Al4V material that in figure 11 has the highest predicted susceptibility of hot spot heating [43].

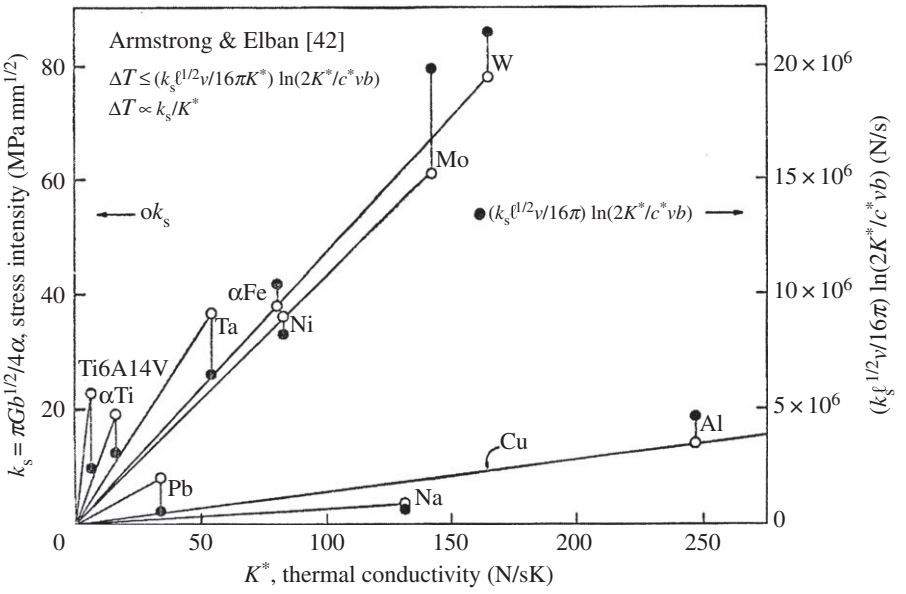

Figure 11. A shear band susceptibility criterion, k_S/K^*, for metals.

6. Discussion

Hopkinson, in his seminal 1914 paper [7], added importantly to the topics of impact and detonation covered in his two earlier publications [2,6]. In [2], Hopkinson begins with discussion of the elastic impact of ivory (billiard) balls and notes the rapid build-up of higher pressures at exceedingly small ball separations and thus leading for balls made of mild steel to much higher plastic flow strengths. Fig. 1 of [2] is a description of the Hertzian elastic contact force between the impacting ivory balls. It is important to know that the high velocity ball penetration described here in figure 5 starts with elastic contact between the ball and target. With modern indentation hardness methods, including nano-indentation hardness testing, the elastic, plastic and cracking behaviours of materials are usefully probed in order to determine the full loading response of any material, including elastic/plastic rebound experiments [44].

By means of hardness testing or conventional tension/compression testing, a reasonable flow stress of copper at ambient temperature and strain rate, say, of approximately $10^{-3}\,s^{-1}$ is approximately 40 MPa that can be raised as shown in figure 4 to approximately 350 MPa through strain hardening at a strain rate of approximately $2 \times 10^4\,s^{-1}$. Figure 6 shows that a higher flow stress of approximately 3 GPa is reached for shock-induced deformation at a plastic strain rate of approximately $8 \times 10^6\,s^{-1}$; and then figure 8 shows a highest flow stress value of approximately 40 GPa is reached at an ICE-determined strain rate of approximately $3 \times 10^4\,s^{-1}$. The increase in flow stress by a factor of 1000 is noteworthy. The same is true for comparison of a higher copper flow stress result obtained as an ICE result at a slower strain rate than the higher one quoted for the lower shock stress. The different physical situations of shock-induced dislocation generation as compared with drag-controlled motion of a resident dislocation density explain the relative standing of the two measurements. The drag coefficient becomes infinite at the shear wave speed.

Figure 12 shows a more recent compilation of shock measurements obtained for copper material and for which the issue of subsequent movement of an enhanced shock-induced density of dislocations has been considered [45]. The results of Swegle & Grady [33] from figure 6 have been added to the figure [46]. The figure also includes a more complete description (on a shear stress basis) of the Follansbee *et al*. [25] results at increasing strain values. The observed increase in strain rate dependence is predicted by equation (4.1) that has been drawn in the figure for the lower stress SHPB results. Equation (3.1), designated as AAZ, is included in the figure for

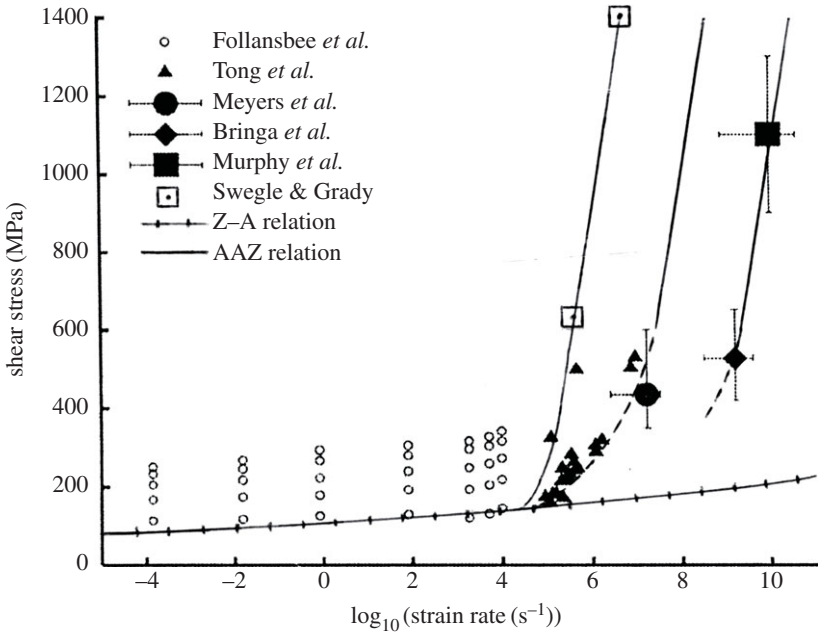

Figure 12. Compilation of additional SHPB and shock results for copper.

the Swegle and Grady results. The same shock dependence is shown at the several shifted positions to include the higher strain rates achieved in other cases. The suggestion was put forward by Armstrong and Zerilli that the greater strain rates, past the Swegle and Grady results, may be primarily attributed to subsequent movement of dislocations within the higher densities generated at the shock fronts. A dislocation density of approximately $10^{18}\,\mathrm{m}^{-2}$ was produced in simulation of both molecular dynamics and X-ray diffraction results on a sub-nanosecond time scale, thus placing dislocations at approximately 1 nm separation along the shock front [47].

The turn-up in the high strain rate dependence of the flow stress for copper has been reported also for a number of other materials, most notably in SHPB results reported for Armco iron material by Ostwaldt *et al*. [48]. A strain rate equal to $9000\,\mathrm{s}^{-1}$ was achieved in material with a grain size of 15 µm. Again, deformation twinning was found to have occurred and the twinning structure was reported to have been fragmented at a small dimensional scale by generation of a high dislocation density. Such twinning has been shown to be relatively more difficult in similar SHPB and shock tests reported for tantalum material. A similar partial Burgers vector twinning explanation was given for the fit of equation (4.1) to the shock results [10]. And a tabulation of Z–A constants for equation (3.1) had been given previously for conventional deformation results obtained on tantalum, including prediction of the uniform strain leading to tensile instability [49]. The information was employed by Pappu & Murr [50] to model the shapes of tantalum material formed into explosively fired projectiles. Agreement has been shown also [50] with Z–A prediction for an upturn of SHPB results reported for tantalum crystal and polycrystal materials [51]. Latest measurements reported for aluminium at very high pressures [52] have been described as well on the same Z–A-type model basis [53].

7. Summary

Bertram Hopkinson deserves much credit for his contributions to starting researches on the combined topics of high rate loading of materials and better understanding of explosive detonations. This article gives some indication of how far the topics have progressed during these past 100 years and provides evidence of the continuing researches. New SHPB systems

continue to be developed and these systems and other dynamic mechanical testing methods and model material performance relationships are being extended to ever higher loading rates and consequent stress levels.

Acknowledgements. Appreciation is expressed to the guest editors for the invitation to participate in the Bertram Hopkinson centenary celebration of the 1914 article. Stephen Walley is thanked especially for providing a number of important reference articles for inclusion in this report.

References

1. Oliver LR, Armstrong RW, Clifton RJ, Kolsky H. 1967 Cleavage of zinc single crystals induced by stress waves. *Nature* **216**, 910. (doi:10.1038/216910a0)
2. Hopkinson B. 1921 The pressure of a blow. [1912] In *The scientific papers of Bertram Hopkinson* (eds JA Ewing, J Larmor), ch. 26, pp. 423–437. Cambridge, UK: Cambridge University Press.
3. Chen Y, Clausen AH, Hopperstad OS, Langseth M. 2011 Application of a split-Hopkinson tension bar in a mutual assessment of experimental tests and numerical predictions. *Int. J. Impact Eng.* **38**, 824–836. (doi:10.1016/j.ijimpeng.2011.05.002)
4. Gerlach R, Kettenbeil C, Petrinic N. 2012 A new split Hopkinson tensile bar design. *Int. J. Impact Eng.* **50**, 63–67. (doi:10.1016/j.ijimpeng.2012.08.004)
5. Armstrong RW, Arnold W, Zerilli FJ. 2009 Dislocation mechanics of copper and iron in high rate deformation tests. *J. Appl. Phys.* **105**, 023511. (doi:10.1063/1.3067764)
6. Hopkinson B. 1921 The effects of the detonation of gun-cotton. [1913] In *The scientific papers of Bertram Hopkinson* (eds JA Ewing, J Larmor), ch. 28, pp. 461–474. Cambridge, UK: Cambridge University Press.
7. Hopkinson B. 1914 A method of measuring the pressure produced in the detonation of high explosives or by the impact of bullets. *Phil. Trans. R. Soc. Lond. A* **213**, 437–456. (doi:10.1098/rsta.1914.0010)
8. Taylor GI. 1948 The use of flat-ended projectiles for determining dynamic yield strength. I. Theoretical considerations. *Proc. R. Soc. Lond. A* **194**, 289–299. (doi:10.1098/rspa.1948.0081)
9. Armstrong RW, Zerilli FJ. 1988 Dislocation mechanics based analysis of material dynamics behavior. *J. Phys. Fr. Colloq.* **49**, 529–534. (doi:10.1051/jphyscol:1988374)
10. Armstrong RW, Arnold W, Zerilli FJ. 2007 Dislocation mechanics of shock-induced plasticity. *Metall. Mater. Trans. A* **38A**, 2605–2610. (doi:10.1007/s11661-007-9142-5)
11. Armstrong RW, Walley SM. 2008 High strain rate properties of metals and alloys. *Int. Mater. Rev.* **53**, 105–128. (doi:10.1179/174328008X277795)
12. Armstrong RW, Zerilli FJ. 1994 Dislocation mechanics aspects of plastic instability and shear banding. *Mech. Mater.* **17**, 319–327. (doi:10.1016/0167-6636(94)90069-8)
13. Armstrong RW, Elban WL. 2006 Materials science and technology aspects of energetic (explosive) materials. *Mater. Sci. Technol.* **22**, 381–395. (doi:10.1179/174328406X84049)
14. Whiffin AC. 1948 The use of flat-ended projectiles for determining dynamic yield stress. II. Tests on various metallic materials. *Proc. R. Soc. Lond. A* **194**, 300–322. (doi:10.1098/rspa.1948.0082)
15. Carrington WE, Gaylor MLV. 1948 The use of flat-ended projectiles for determining dynamic yield stress. III. Changes in microstructure caused by deformation under impact at high-striking velocities. *Proc. R. Soc. Lond. A* **194**, 323–331. (doi:10.1098/rspa.1948.0083)
16. Johnson GR, Cook WH. 1983 A constitutive model and data for metals subjected to large strains, high strain rates and high temperatures. In *Proc. 7th Int. Symp. on Ballistics, The Hague, The Netherlands, 19–21 April 1983*, pp. 541–547. Washington, DC: American Defense Preparedness Association.
17. Zerilli FJ, Armstrong RW. 1987 Dislocation-mechanics-based constitutive equations for material dynamics calculations. *J. Appl. Phys.* **61**, 1816–1825. (doi:10.1063/1.338024)
18. Hall EO. 1951 The deformation and ageing of mild steel: III. Discussion of results. *Proc. Phys. Soc. Lond.* **B64**, 747–753. (doi:10.1088/0370-1301/64/9/303)
19. Petch NJ. 1953 The cleavage strength of polycrystals. *J. Iron Steel Inst.* **174**, 25–29.
20. Armstrong RW. 1983 The yield and flow stress dependence on polycrystal grain size. In *Yield, flow and fracture of polycrystals* (ed. TN Baker), pp. 1–31. London, UK: Applied Science Publishers.
21. Armstrong RW, Roberson L, Speich GR. 1988 Analysis of brittle: ductile transition temperatures for controlled-rolled, microalloyed, C-Mn based steels. In *Processing*

microstructure and properties of HSLA steels (ed. AJ DeArdo), pp. 305–315. Pittsburgh, PA: The Metallurgical Society, AIME.
22. Zerilli FJ, Armstrong RW. 1988 Dislocation-mechanics-based constitutive relations for material dynamics modeling: slip and deformation twinning in iron. In *Shock waves in condensed matter 1987* (eds SC Schmidt, NC Holmes), pp. 273–276. Oxford, UK: Elsevier Science.
23. McKirgan JB. 1990 Microstructurally-based EPIC simulations of Taylor impact tests. MSc thesis, University of Maryland, College Park, MD, USA.
24. Taylor GI. 1938 Plastic strain in metals. *J. Inst. Met.* **62**, 307–324.
25. Follansbee PS, Regazzoni G, Kocks UF. 1984 The transition in drag-controlled deformation in copper at high strain rates. In *Mechanical properties at high rates of strain* (ed J. Harding). Conference Series, no. 70, pp. 71–80. London, UK: Institute of Physics.
26. Rodriguez P. 2004 Grain size dependence of the activation parameters for plastic deformation: influence of crystal structure, slip system, and rate controlling dislocation mechanism. *Metall. Mater. Trans. A* **35A**, 2697–2705. (doi:10.1007/s11661-004-0215-4)
27. Volterra E. 1948 Alcuni risultati di prove dinamiche sui materiali. *La Revista del Nuovo Cimento* **IV**, 1–28.
28. Cai MC, Shi HJ, Yu T. 2011 A dislocation-based constitutive description of strain rate effect on the deformation resistance of metals. *J. Mater. Sci.* **46**, 1087–1094. (doi:10.1007/s10853-010-4877-6)
29. Fan Y, Osetsky YN, Yip S, Yildiz B. 2012 Onset mechanism of strain-rate-induced flow stress upturn. *Phys. Rev. Lett.* **109**, 135503. (doi:10.1103/PhysRevLett.109.135503)
30. Murr LE. 2012 Correlating impact related residual microstructures through 2D computer simulations and microindentation hardness mapping. *Mater. Sci. Technol.* **28**, 1108–1126. (doi:10.1179/1743284712Y.0000000008)
31. Quinones SA, Murr LE. 1998 Correlations of computed simulations with residual hardness mapping and microstructural observations of high velocity and hypervelocity impact craters in copper. *Phys. Stat. Sol. A* **166**, 763–789. (doi:10.1002/(SICI)1521-396X(199804)166:2<763::AID-PSSA763>3.0.CO;2-9)
32. Armstrong RW. 1992 Roles possibles des dislocations dans les detonations par shoc. (trad. J. Boileau). *Revue Scientifique et Technique de la Defense* **16**, 161–164.
33. Swegle JW, Grady DE. 1985 Shock viscosity and the prediction of shock wave rise times. *J. Appl. Phys.* **58**, 692–701. (doi:10.1063/1.336184)
34. Arnold W. 1992 *Dynamisches Werkstoffverhaltern von Armco-Eisen Stosswellbelastung*, vol. 5, pp. 1–247. Duesseldorf, Germany: Fortschrittberichte VDI.
35. Jarmakani H, McNaney JM, Kad B, Orlikowski D, Nguyen JH, Meyers MA. 2007 Dynamic response of single crystalline copper subjected to quasi-isentropic, gas gun loading. *Mater. Sci. Eng. A* **463**, 249–262. (doi:10.1016/j.msea.2006.09.118)
36. Head AK. 1973 Dislocation group dynamics VI. The release of a pile-up. *Philos. Mag.* **27**, 531–539. (doi:10.1080/14786437308219229)
37. Heavens SN, Field JE. 1974 Ignition of a thin layer of explosive by impact. *Proc. R. Soc. Lond. A* **338**, 77–93. (doi:10.1098/rspa.1974.0074)
38. Armstrong RW, Coffey CS, Elban WL. 1982 Adiabatic heating at a dislocation pile-up avalanche. *Acta Metall.* **30**, 2111–2118. (doi:10.1016/0001-6160(82)90131-6)
39. Armstrong RW, Elban WL. 2010 From intermolecular shearing to composite behavioral predictions for initiation of energetic materials. In *14th Int. Detonation Symp., Coeur d' Alene, ID, USA, 11–16 April 2010* (eds S. Peiris, C. Boswell, B. Asay), pp. 1430–1439. Arlington, VA: Office of Naval Research.
40. Armstrong RW, Bardenhagen SG, Elban WL. 2012 Deformation-induced hot spot consequences of AP and RDX crystal hardness measurements. *Int. J. Energ. Mater. Chem. Comb.* **11**, 413–425. (doi:10.1615/IntJEnergeticMaterialsChemProp.2013005348)
41. Armstrong RW. 2009 Dislocation mechanics aspects of energetic material composites. *Rev. Adv. Mater. Sci.* **19**, 13–40.
42. Armstrong RW, Elban WL. 1989 Temperature rise at a dislocation pile-up breakthrough. *Mater. Sci. Eng.* **A122**, L1–L3. (doi:10.1016/0921-5093(89)90642-4)
43. Holt WH, Mock Jr W, Soper WG, Coffey CS, Ramachandran V, Armstrong RW. 1993 Reverse-ballistic shear plug formation and displacement in Ti6Al4V alloy. *J. Appl. Phys.* **73**, 3753–3759. (doi:10.1063/1.354053)

44. Armstrong RW, Elban WL, Walley SM. 2013 Elastic, plastic, and cracking aspects of the hardness of materials. *Int. J. Mod. Phys. B* **27**, 1330004. (doi:10.1142/S0217979213300041)
45. Armstrong RW, Zerilli FJ. 2010 Shock-induced rates of straining of copper. *J. Phys. D Appl. Phys.* **43**, 492002. (doi:10.1088/0022-3727/43/49/492002)
46. Murphy WJ *et al*. 2010 The strength of single crystal copper under uniaxial shock compression at 100 GPa. *J. Phys. Condens. Matter* **22**, 065404. (doi:10.1088/0953-8984/22/6/065404)
47. Bringa EM, Rosolankova K, Rudd RE, Remington BA, Wark JS, Duchaineau M, Kalantar DH, Hawreliak J, Belak J. 2006 Shock deformation of face-centered-cubic metals on subnanosecond time scales. *Nat. Mater.* **5**, 805–809. (doi:10.1038/nmat1735)
48. Ostwaldt D, Klepaczko JR, Klimanek P. 1997 Compression testing of polycrystalline α-iron up to high strains over a large range of strains. *J. Phys. IV* **7**, 385–390. (doi:10.1051/jp4:1997367)
49. Zerilli FJ, Armstrong RW. 1990 Description of tantalum deformation behavior by dislocation mechanics based constitutive relations. *J. Appl. Phys.* **68**, 1580–1591. (doi:10.1063/1.346636)
50. Pappu S, Murr LE. 2002 Hydrocode and microstructural analysis of explosively formed penetrators. *J. Mater. Sci.* **37**, 333–348. (doi:10.1023/A:1013665108127)
51. Rittel D, Silva ML, Poon B, Ravichandran G. 2009 Thermomechanical behavior of single crystal tantalum in the static and dynamic regime. *Mech. Mater.* **41**, 1323–1329. (doi:10.1016/j.mechmat.2009.08.001)
52. Crowhurst JC, Armstrong MR, Knight KB, Zaug JM, Behymer EM. 2011 Invariance of the dissipative action at ultrahigh rates above the strong shock threshold. *Phys. Rev. Lett.* **107**, 144302. (doi:10.1103/PhysRevLett.107.144302)
53. Armstrong RW. 2014 Dislocation mechanics of high rate deformations. In *Proc. Plasticity '14: Multi-scale Modeling and Plasticity Characterization of Advanced Materials* (eds AS Khan, H-Y Yu), pp. 133–135. Fulton, MD: NEAT Press.